Supporting Information for "Fast warming of the surface ocean under a climatological scenario"

Q. Jamet[1] *, W. K. Dewar[1], N. Wienders[1]and B. Deremble[2]

[1]Department of Earth, Ocean and Atmospheric Science, the Florida State University, Tallahassee, Florida

[2]Laboratoire de Météorologie Dynamique, Paris, France

Contents of this file

Corresponding author: Q. Jamet, Department of Earth, Ocean and Atmospheric Science, the Florida State University, Tallahassee, Florida. (qjamet@fsu.edu)

*The Florida State University, 117 N

Woodward Avenue, Tallahassee, FL

32306-4320.

Model Configuration The configuration used in this study is based on the MIT general circulation model (MITgcm Marshall et al., 1997) deployed in a regional configuration of the North Atlantic from 20°S to 55°N with a horizontal resolution of $\frac{1}{4}^\circ$ and vertical resolution ranging from 6 m near the surface to 250 m near the bottom (i.e. 46 levels). Although mesoscale eddies are partially resolved at $\frac{1}{4}^\circ$ horizontal resolution, their impacts are also parametrized as an advective process (Gent and McWilliams, 1990) and an isopycnal diffusion (Redi, 1982) with a transfer coefficient of 1200 m^2 s^{-1} for both processes. We use the non-local K-Profile Parametrization (KPP) scheme of Large et al. (1994) with a critical Richardson number of 0.3 to parametrize the vertical mixing in the upper ocean boundary layer. The oceanic initial conditions are derived from the spun-up oceanic state of the $\frac{1}{12}^\circ$ horizontal resolution global configuration of Sérazin et al. (2015), linearly interpolated on our model grid. At the northern boundary (55°N), southern boundary (20°S) and at the Strait of Gibraltar, we apply the boundary conditions from the $\frac{1}{12}^\circ$ horizontal resolution global configuration of Sérazin et al. (2015), linearly interpolated on our model grid.

All experiments start from the initial oceanic state of the $\frac{1}{12}^\circ$ global ocean-only ORCA12.L46-MJM88 simulation interpolated on our $\frac{1}{4}^\circ$ model grid. The initial oceanic state of this global ocean-only simulation has been made as a 5-day long run under realistic forcing starting at rest with initial temperature and salinity conditions taken from a monthly climatology derived from a merge of the Levitus 1998 climatology (see Molines et al., 2014, for more details).

Atmospheric Boundary Layer Model: CheapAML Two of the experiments discussed in the main text (AML_FULL and AML_CLIM) make use of the atmospheric boundary layer model CheapAML (Deremble et al., 2013). Relevant informations about this model are given here, but the reader is referred to the original paper of Deremble et al. (2013) for a broader description. This model aims at representing a dynamical atmospheric boundary layer in order to increase the consistency of air-sea interactions. The main assumption of this framework is that the atmospheric winds are the least sensitive reanalysis variables to the ocean surface structure. They are thus prescribed and air-sea feedbacks induced by oceanic surface currents or SST fronts on winds are not considered here. The remaining atmospheric variables, i.e. temperature and relative humidity, are advected by the winds and are modified by the air-sea fluxes. Over the ocean, the temporal evolution of these atmospheric variables is computed following a forced advection-diffusion equation

$$(\partial_t s + \nabla(\mathbf{u}s)) = -\partial_z F + \nabla.(K\nabla s)\,, \tag{1}$$

where s is the atmospheric temperature or relative humidity, $\mathbf{u}$ is the non-divergent atmospheric winds, F are fluxes that enter or leave the boundary layer at the top and at the bottom (the height of the boundary layer $h = 1000$ m is taken as constant in time and space), and $K = 1000$ m^2 s^{-1} is the atmospheric diffusivity. The components of the net heat fluxes at the bottom of the boundary layer model (Q_{net}, positive upward) are: (i) prescribed downward shortwave radiation, (ii) longwave radiation (the sum of prescribed downward longwave radiations and outgoing longwave radiations), and (iii) latent and sensible heat fluxes, computed with the bulk formula of the Coupled Ocean-Atmosphere

Response Experiment, version 3 (COARE3, Fairall et al., 2003). The atmospheric variables prescribed in CheapAML, i.e. solar shortwave and downward longwave radiation, precipitation, atmospheric temperature and relative humidity over land and zonal and meridional wind components, are applied every 6 hours and derived from the Drakkar forcing set (see below). Over land, temperature and relative humidity are relaxed toward the reanalysis prescribed values.

All experiments have been run with prescribed downward longwave radiations, such that changes in atmospheric temperature are not accounted for in the radiative budget. The net longwave radiation at the air-sea interface is computed simply as $LW_{net} = LW_{ocn} - LW_{atm}^{presc.}$. We have an additional experiment for AML_CLIM (referred to as AML_CORR_LW) where the warmer atmospheric temperature has been included in the radiative balance such that the net longwave radiation at the ocean surface becomes:

$$LW_{net} = LW_{ocn} - LW_{atm}^{presc.} - \frac{\epsilon * \sigma}{2} * \left[4 * (T_A^{dfs})^3 * \Delta T + 6 * (T_A^{dfs})^2 * \Delta T^2 + T_A^{dfs} * \Delta T^3 + \Delta T^4\right] \quad (2)$$

with $\epsilon = 0.90$ the emissivity of the atmosphere, $\sigma = 5.67\ 10^{-8}$ W m^{-2} K^{-4} the Stefan Boltzmann constant, T_{dfs} the DFS4.4 atmospheric temperature associated with the prescribed atmospheric downward longwave radiations and $\Delta T = T_{aml} - T_{dfs}$ where T_{aml} is the atmospheric temperature computed by CheapAML. The impact of the modified net longwave radiation is to warm by few additional degrees the ocean surface since the warming atmosphere now emits stronger downward longwave radiations back to the surface (Fig. S3, green line).

Atmospheric Data We get all atmospheric variables from the Drakkar forcing set DFS4.4. This product is developed by the DRAKKAR project and provide consistent global forcing datasets based on a combination of the ERA-40 reanalysis and satellite observations. The version 4.4 differs from the version 4 (DFS4 Brodeau et al., 2010) only after 31 December 2001, where ERA-Interim is used instead of the ECMWF analysis (some additional details are given in Molines et al., 2014). The atmospheric variables from DFS4.4 used in CheapAML include: 6-hourly 10-meter zonal and meridional wind components; 2-meter air temperature and relative humidity; and daily downward longwave and solar shortwave radiation. The net longwave radiation flux at the ocean surface is computed as the difference between the prescribed downward atmospheric longwave radiation and the upward longwave radiation associated with the ocean surface temperature ($\epsilon\sigma SST^4$). The albedo is thus implicitly included in this computation. To estimate the fraction of the solar shortwave radiation absorbed by the ocean surface, a correction on the prescribed radiative flux is required by considering ocean surface albedo. This is not currently accounted for in CheapAML, such that the prescribed shortwave radiation has to account for that correction. Such a correction has however been omitted in this study. The absolute shortwave radiative forcing at the surface ocean is thus overestimated by about 5% in all our experiments. This is not expected to impact at a leading order the comparison made between experiments since this omission is identical in all simulations.

From the daily values of the solar shortwave radiation, we reconstruct a diurnal cycle such that the short waves are zero at 6 am and 12 am, and the daily values are doubled at 12 pm and 6 pm. Daily downward longwave radiation is linearly extrapolated in time to

6-hourly field. We also use daily precipitations from DFS5.2 (Dussin and Barnier, 2013; Dussin et al., 2016) because it has a better time resolution in this data set (monthly fields in DFS4.4). Precipitations are also linearly extrapolated to 6-hourly fields. Note that due the lack of observations for radiative fluxes and precipitations before 1979, those fluxes are extended backward in time in the DFS by a yearly repeated seasonally varying climatology computed from an ensemble average of all years days for the period 1979-2012. All these atmospheric fields are linearly interpolated onto our regular $\frac{1}{4}^\circ$ horizontal resolution model grid.

Normal year forcing experiment We detail here the additional experiment AML_NY forced by a 'normal' year surface forcing (Large and Yeager, 2004). This forcing consists in repeating every year the forcing of a given year. With this forcing, we filter out interannual and longer atmospheric variability in the surface forcing but we keep the synoptic atmospheric variability. We have conducted this additional experiment using the winter 2003-2004. This period has been found to be the most 'normal' winter in term of low-frequency atmospheric variability in the 1958-present time frame, with a number of occurrences of the Atlantic Ridge weather regime the closest to the 1958-2012 mean. We have placed the focus on the Atlantic Ridge weather regime to identify a normal year since it has been shown to be the weather regime the most correlated to the North Atlantic subtropical Sea Surface Height interannual variability (Barrier et al., 2013). The occurrence of this weather regime has been found to induce a northward shift of the wind-stress curl, altering the Sverdrup balance and the westward propagating Rossby waves. Such processes are of importance for the low-frequency variability of the North Atlantic

large-scale circulation such as the Atlantic Meridional Overturning Circulation (AMOC). Note that the year 2003 has already been considered as 'normal' in terms of long-term patterns of the North Atlantic Oscillation (NAO, Chassignet and Xu, 2017), providing further confidence. We opt to define our 'normal' year forcing from August 2003 to July 2004 in order to preserve the winter time synoptic atmospheric dynamics (contrarily to Large and Yeager (2004) and Chassignet and Xu (2017)). August-July is found to be the period of the year where the differences in wind speed between 2003 and 2004 are the smallest (Fig. S1). A 30 days linear transition is used to avoid abrupt changes in the forcing.

Heat Budget Following Peter et al. (2006), we have performed a heat budget within the mixed layer and in a box at the center of the subtropical gyre where the SST difference is the largest. We provide here a complete description of the terms included in this budget. By integrating the equation for temperature:

$$D_t T = -Q_{net} - \nabla \left(\mathbf{K} \nabla T \right), \tag{3}$$

over the depth of the mixed layer $h(x, y, t)$, taken here as the depth of the mixed layer computed by the KPP parameterization, we can derive an equation for the temporal temperature tendency within the mixed layer $\partial_t \langle T \rangle$ as follows:

$$\partial_t \langle T \rangle = - \langle \mathbf{u}.\nabla T \rangle - \frac{Q_{net}}{\rho_0 C_p h} + \langle \nabla_h (K_h . \nabla_h T) \rangle - \frac{1}{h} K_z \partial_z T|_{z=-h} - \frac{1}{h} \partial_t h (SST - T|_{z=-h}). \tag{4}$$

The different notations in the upper equations are: $D_t = (\partial_t + \nabla)$ the material derivative; $\nabla = \partial_x \mathbf{i} + \partial_y \mathbf{j} + \partial_z \mathbf{k}$ the 3-dimensional gradient operator and ∇_h its horizontal component; $< \cdot >= \frac{1}{h} \int_{-h}^{0} \cdot dz$ a vertical integration operator; $\mathbf{u}$ the 3-dimensional velocity field;

Q_{net} (positive upward) the net heat fluxes at the air-sea interface; $\rho_0 = 10^3$ kg m^{-3} the reference density for sea water; $C_p = 4.1655 \times 10^3$ J kg^{-1} K^{-1} its heat capacity. The 3-dimensional temperature diffusion operator $\mathbf{K}$ is separated in a horizontal component K_h, taken as $K_h = 200$ m^2 s^{-1} to follow the coefficient used in our configuration, and a vertical component K_z including a background vertical diffusivity of 10^{-5} m^2 s^{-1} and the estimation made by the KPP scheme in the mixed layer.

Fig. S5 shows the contribution of the surface heat fluxes $-\frac{Q_{net}}{\rho_0 C_p h}$ (top right) and the vertical diffusion at the bottom of the mixed layer $\frac{1}{h} K_z \partial_z T|_{z=-h}$ (bottom left) for the total temperature tendency $\partial_t \langle T \rangle$ (top left). The other terms are at least one order of magnitude smaller. For comparison, the residual $resid. = \partial_t \langle T \rangle + \frac{Q_{net}}{\rho_0 C_p h}$ is shown on the bottom right panel.

References

Barrier, N., Treguier, A.-M., Cassou, C., and Deshayes, J. (2013). Impact of the winter north-atlantic weather regimes on subtropical sea-surface height variability. *Climate dynamics*, *41*(5-6), 1159–1171.

Brodeau, L., Barnier, B., Treguier, A.-M., Penduff, T., and Gulev, S. (2010). An era40-based atmospheric forcing for global ocean circulation models. *Ocean Modelling*, *31*(3-4), 88–104.

Chassignet, E. P., and Xu, X. (2017). Impact of horizontal resolution (1/12 to 1/50) on gulf stream separation, penetration, and variability. *Journal of Physical Oceanography*, *47*(8), 1999–2021.

Deremble, B., Wienders, N., and Dewar, W. (2013). Cheapaml: A simple, atmospheric

boundary layer model for use in ocean-only model calculations. *Mon. Wea. Rev.*, *141*(2), 809–821.

Dussin, R., and Barnier, B. (2013). *The making of DFS 5.1. Drakkar Project Rep.* [available online at http://www.drakkar-ocean.eu/publications/reports/dfs5-1-report].

Dussin, R., Barnier, B., Brodeau, L., and Molines, J. (2016). The making of the drakkar forcing set dfs5. *DRAKKAR/MyOcean Rep. 01–04*, *16*.

Fairall, C., Bradley, E. F., Hare, J., Grachev, A., and Edson, J. (2003). Bulk parameterization of air–sea fluxes: Updates and verification for the coare algorithm. *J. Clim.*, *16*(4), 571–591.

Gent, P. R., and McWilliams, J. C. (1990). Isopycnal mixing in ocean circulation models. *J. Phys. Oceanogr.*, *20*(1), 150–155.

Large, W. G., McWilliams, J. C., and Doney, S. C. (1994). Oceanic vertical mixing: A review and a model with a nonlocal boundary layer parameterization. *Rev. Geophys.*, *32*(4), 363–403.

Large, W. G., and Yeager, S. G. (2004). Diurnal to decadal global forcing for ocean and sea-ice models: the data sets and flux climatologies.

Marshall, J., Adcroft, A., Hill, C., Perelman, L., and Heisey, C. (1997). A finite-volume, incompressible Navier Stokes model for studies of the ocean on parallel computers. *J. Geophys. Res.*, *102*(C3), 5753–5766.

Molines, J.-M., Barnier, B., Penduff, T., Treguier, A., and Le Sommer, J. (2014). *Orca12. l46 climatological and interannual simulations forced with dfs4. 4: Gjm02 and mjm88. drakkar group experiment rep* (Tech. Rep.). GDRI-

DRAKKAR-2014-03-19, 50 pp.[Available online at http://www. drakkar-ocean. eu/publications/reports/orca12_reference_experiments_2014.].

Peter, A.-C., Le Hénaff, M., Du Penhoat, Y., Menkes, C. E., Marin, F., Vialard, J., ... Lazar, A. (2006). A model study of the seasonal mixed layer heat budget in the equatorial atlantic. *Journal of Geophysical Research: Oceans*, *111*(C6).

Redi, M. H. (1982). Oceanic isopycnal mixing by coordinate rotation. *J. Phys. Oceanogr.*, *12*(10), 1154–1158.

Sérazin, G., Penduff, T., Grégorio, S., Barnier, B., Molines, J.-M., and Terray, L. (2015). Intrinsic variability of sea level from global ocean simulations: Spatiotemporal scales. *J. Clim.*, *28*(10), 4279–4292.

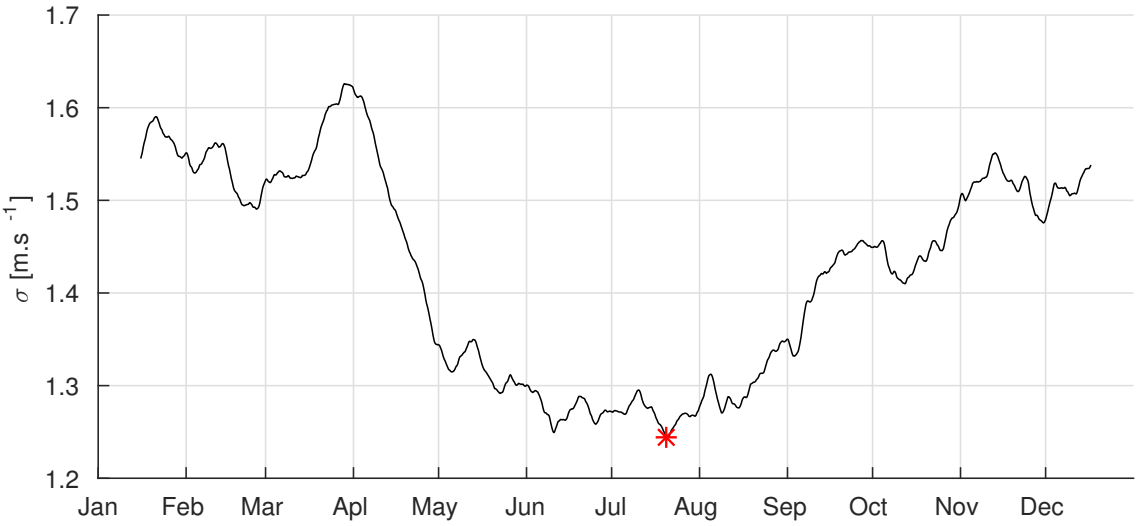

Figure S1. Spatially averaged standard deviation of wind speed between the year 2003 and 2004 as a function of time. Results have been low-pass filtered with a monthly moving mean. The red cross indicates the minimum of standard deviation.

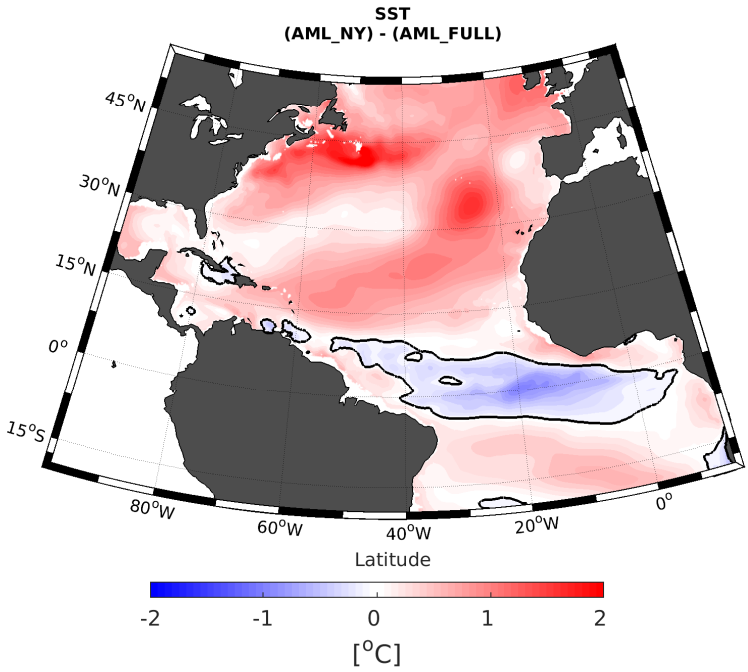

Figure S2. Yearly averaged SST difference between the AML_NY and the AML_FULL experiments for the year 1963. Note the difference in colorbar with Fig. 2 in the main text.

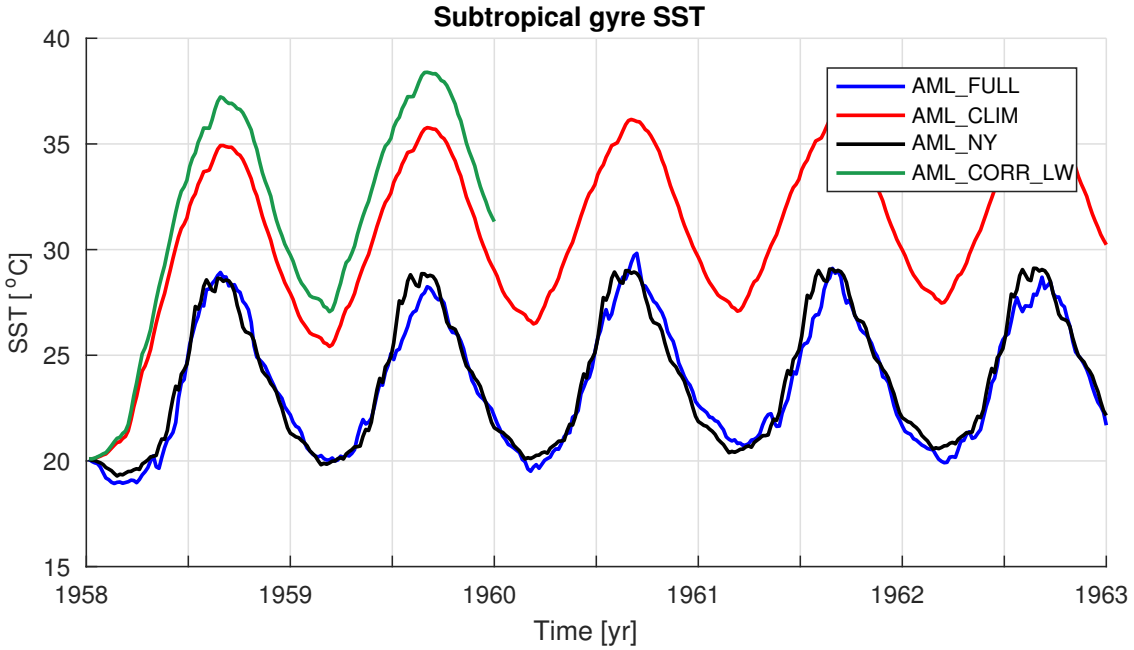

Figure S3. Time series of the spatially averaged SST in the subtropical gyre (as in Fig. 2) for the two additional experiments AML_NY (black) and AML_CORR_LW (green). Also shown are the two experiments AML_FULL (blue) and AML_CLIM (red) for respective comparisons. The experiment AML_NY has been integrated for 5 years, and the experiment AML_CORR_LW for 2 years.

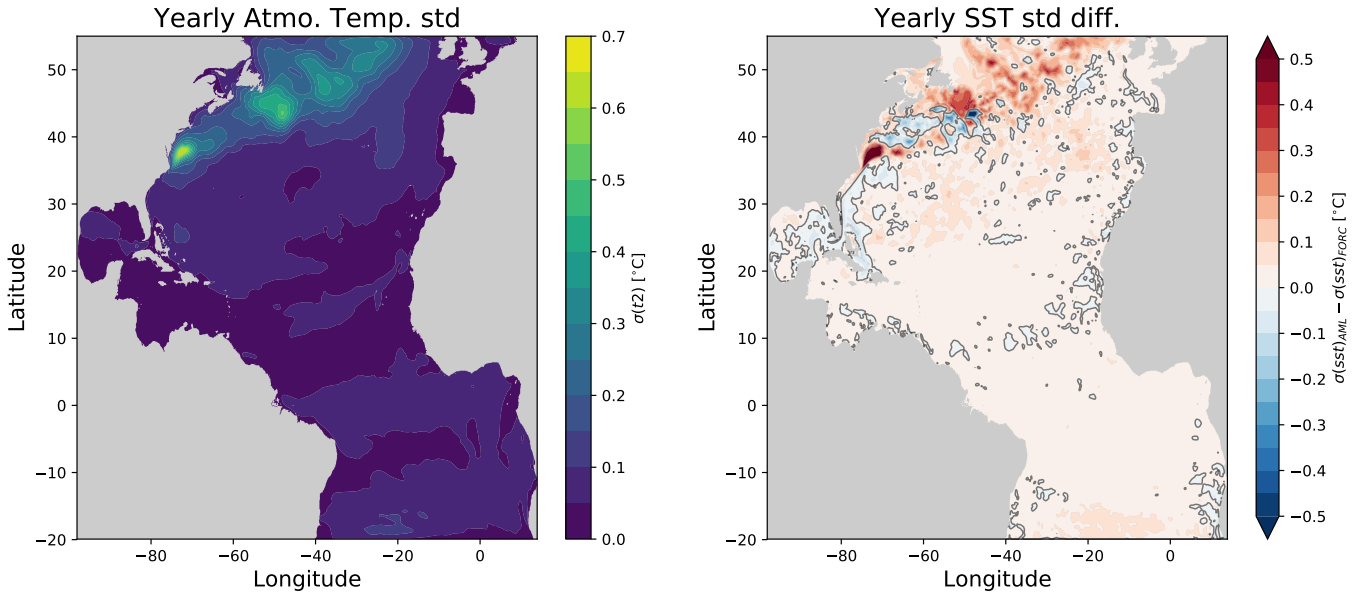

Figure S4. (Left) Standard deviation of yearly averaged atmospheric temperature computed by the atmospheric boundary layer model in an identical North Atlantic regional configuration than AML_NY (same ocean model formulation coupled to CheapAML and using the same 'normal' year forcing), but run for 50 years (1963-2012) with a horizontal resolution of $\frac{1}{12}^{\circ}$. (Right) Standard deviation difference of yearly averaged Sea Surface Temperature between the 50-yr long, high resolution simulation coupled to CheapAML and the same 50-yr long, high resolution simulation driven by prescribed 'normal' year atmospheric forcing (i.e. wind, atmospheric surface air temperature and humidity).

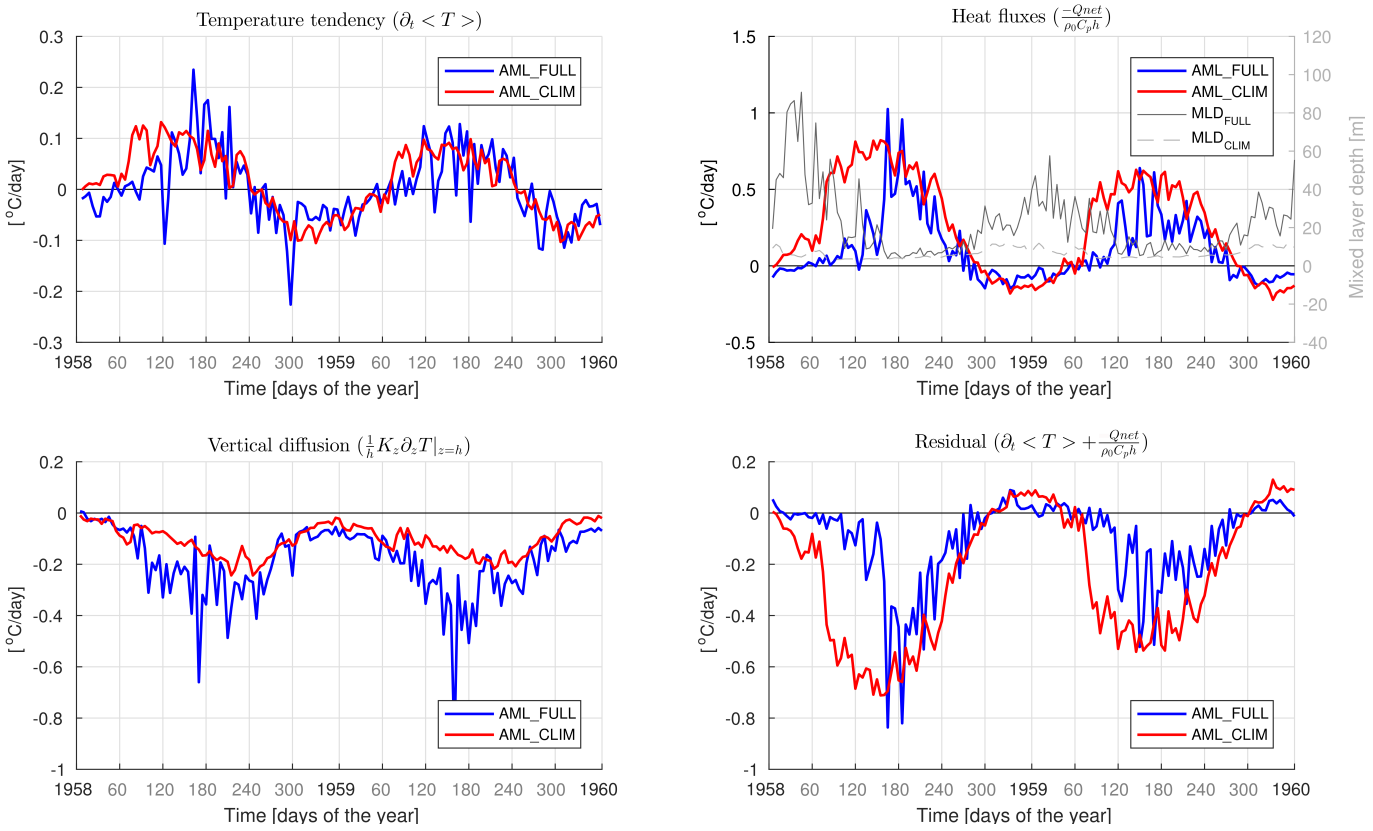

Figure S5. Contribution of the net heat fluxes $-\frac{Q_{net}}{\rho_0 C_p h}$ (top right, Q_{net} positive upward) and the vertical diffusion at the bottom of the mixed layer $\frac{1}{h} K_z \partial_z T|_{z=-h}$ (bottom left) for the temperature tendency $\partial_t \langle T \rangle$ (top left) within the mixed layer for AML_FULL (blue) and AML_CLIM (red). The total contribution of dissipative, advective and entrainment terms is computed as a residual $resid. = \partial_t \langle T \rangle + \frac{Q_{net}}{\rho_0 C_p h}$ (bottom right). Gray lines on top right panel represent the depth of the mixed layer, with the associated axe on the right. The budget is made at the center of the subtropical gyre (green box of Fig. 2) following Eq. (4).